

HIGH GAS FRACTION IN A CO-SELECTED MAIN-SEQUENCE GALAXY AT $Z > 3$

AVANI GOWARDHAN,¹ DOMINIK RIECHERS,¹ RICCARDO PAVESI,¹ EMANUELE DADDI,² HELMUT DANNERBAUER,^{3,4}
ROBERTO NERI⁵

¹*Department of Astronomy, Cornell University, Ithaca, NY 14853, USA*

²*Irfu/Service d'Astrophysique, CEA Saclay, Orme des Merisiers, F- 91191 Gif sur Yvette, France*

³*Instituto de Astrofísica de Canarias (IAC), E-38205 La Laguna, Tenerife, Spain*

⁴*Universidad de La Laguna, Dpto. Astrofísica, E-38206 La Laguna, Tenerife, Spain*

⁵*Institut de Radioastronomie Millimétrique, 300 rue de la Piscine, F-38406, Saint-Martin d'Hères, France*

ABSTRACT

We report NOthern Extended Millimetre Array (NOEMA) observations of warm molecular gas traced by CO(5–4) in a $z \sim 3.2$ gas-rich main-sequence galaxy (MS), initially serendipitously detected in CO(3–2) emission in ‘blind’ deep NOEMA observations. Our target shows a gas excitation consistent with that seen in $z \sim 1.5$ MS galaxies ($L'_{\text{CO}(5-4)}/L'_{\text{CO}(3-2)} = 0.41 \pm 0.14$), albeit toward the low end, as well as a similar star formation efficiency based on the CO(3–2) line luminosity and the L_{IR} . However, it shows a high molecular gas fraction ($f_{\text{gas}} = 0.9 \pm 0.2$) as compared to $z \sim 1.5$ MS galaxies ($f_{\text{gas}} \sim 0.42$), consistent with a cosmologically increasing gas fraction beyond $z \gtrsim 3$ and our current understanding of scaling relations between z , f_{gas} , the stellar mass M_* , and the specific star formation rate sSFR. Our results are consistent with recent findings by the COLDz and ASPECS molecular line scan surveys and suggest that deep searches for CO emission are a powerful means to identify gas-rich, star-forming galaxies at high redshift.

1. INTRODUCTION

Observations of molecular gas - the fuel for star formation - in sizable galaxy samples at high- z are essential to understanding the onset and evolution of the peak epoch of cosmic star formation and stellar mass assembly at $z \sim 1 - 3$ (see Carilli & Walter 2013, for a review). Star-forming galaxies (SFGs) at all cosmic epochs show a redshift-modulated correlation between the stellar mass and the star-formation rate (SFR) - the galaxy main-sequence - suggesting that the bulk of star formation takes place in quasi-steady state, with galaxies undergoing short-lived starburst activity lying significantly above the galaxy main-sequence at any redshift (e.g. Rodighiero et al. 2011; Speagle et al. 2014). Observations of the molecular gas traced by CO as well as dust-based measurements of the total gas and dust mass suggest that the observed increase in star-formation rates in high- z SFGs is driven concurrently by increasing gas fraction (f_{gas}) and star-formation efficiency (SFE) (e.g. Tacconi et al. 2013; Genzel et al. 2015; Scoville et al. 2016; Pavese et al. 2018). However, while there is a general agreement on the evolution of the molecular gas fraction and specific star formation rate (sSFR) up to $z \sim 2$, there is considerable debate about its evolution beyond that epoch. While some studies find a continuing increase in the molecular gas fraction at $z \gtrsim 3$ (Tan et al. 2013; Dessauges-Zavadsky et al. 2015, 2017), as expected from theoretical models (e.g. Obreschkow & Rawlings 2009; Lagos et al. 2011), other measurements indicate a plateauing or even a decline of the molecular gas fraction at the highest redshifts (e.g. Saintonge et al. 2013; Troncoso et al. 2014; Béthermin et al. 2015; Dessauges-Zavadsky et al. 2015; Schinnerer et al. 2016). CO line stacking of 78 galaxies at a mean redshift of $z \sim 2.4$ also shows a lower molecular gas fraction than expected for massive main-sequence galaxies (Pavese et al. 2018). This disagreement can be attributed to the scarcity of molecular gas detections in MS galaxies at $z \gtrsim 3$. CO detections in SFGs at $z \gtrsim 3$ are currently largely restricted to highly lensed systems (magnified $30-60\times$ Coppin et al. 2007; Riechers et al. 2010; Saintonge et al. 2013; Dessauges-Zavadsky et al. 2017). Searches in unlensed Lyman-Break galaxies (LBGs) at $z \sim 3$ have had limited success, with only two detections to date (Magdis et al. 2012; Tan et al. 2013; Magdis et al. 2017).

Observing both low- J and high- J CO lines in high- z SFGs is important as they trace the cold and warm molecular gas phases respectively. While CO Spectral Line Energy Distributions (SLEDs) have been studied in FIR-bright submillimeter galaxies (SMGs) and quasars at high- z (e.g. Weiß et al. 2005; Riechers et al. 2006;

Weiß et al. 2007; Riechers et al. 2011a,b; Danielson et al. 2011; Riechers et al. 2013; Bothwell et al. 2013; Yang et al. 2017; Strandet et al. 2017), these systems are undergoing intense star-formation, have small gas depletion timescales (Yang et al. 2017), and are unlikely to be representative of MS galaxies. The CO SLED has been only sparsely sampled for more ‘normal’ high- z star-forming galaxies, with observations limited to four BzK galaxies at $z \sim 1.5$ (Daddi et al. 2015) and one lensed source at $z \sim 3.6$ (Dessauges-Zavadsky et al. 2017). While low- J ($J_{\text{upper}} = 1, 2, 3$) CO line ratios in these systems resemble those of star-forming galaxies in the local universe, CO(5-4) observations reveal the presence of an additional, warmer molecular gas component, demonstrating the necessity of sampling the CO SLED at multiple J s to accurately probe ISM properties (Daddi et al. 2015).

We here present observations of CO(5-4) emission in EGSIRAC J141912.03+524924.0 (hereafter EGS141912), a gas-rich MS galaxy at $z \sim 3.2$, detected serendipitously in CO(3-2) emission (Gowardhan et al. 2017, hereafter G17). Our new observations confirm the target redshift and provide some of the first constraints on the molecular gas excitation and star formation efficiency in $z > 3$ MS galaxies.

The paper is organized as follows: we present the observations in § 2 and the spectral energy distribution (SED) fitting in § 3. In § 4 and § 5, we discuss our results and conclusions. We use a Λ CDM cosmology, with $H_0 = 71 \text{ km s}^{-1} \text{ Mpc}^{-1}$, $\Omega_M = 0.27$, and $\Omega_\Lambda = 0.73$ (Spergel et al. 2007).

2. OBSERVATIONS

2.1. CO observations

NOEMA observations of the CO(5-4) line ($\nu_{\text{rest}} = 576.26793 \text{ GHz}$) in EGS141912 were conducted in April 2017 (Program ID W16DR), with 8 antennas in the compact D configuration, for a total on-source time of 9.2 hours split across two tracks. Weather conditions were good for both tracks, with a precipitable water vapor (pwv) of 2 - 15 mm, with most of the observations taken in good weather. 3C273 was used as the absolute flux calibrator, and the source J1418+546 was used for phase and bandpass calibration. The WideX correlator (bandwidth $\sim 3.6 \text{ GHz}$) was tuned to a frequency of 136.605 GHz. Observations were carried out in a dual polarization mode, with a binned spectral resolution of $\sim 2.5 \text{ MHz}$ ($\sim 5.5 \text{ km s}^{-1}$ at 136 GHz). All observations were calibrated using the IRAM PdBI data reduction pipeline in CLIC (Continuum and Line Interferometer Calibration), with subsequent additional flagging by hand. The reduced visibility data were imaged

in the software MAPPING, using the tasks UV_MAP and CLEAN, using natural baseline weighting and the Hogbom cleaning algorithm. The final synthesized beam size is $3.''0 \times 2.''5$. The rms noise in the cube is $1.0 \text{ mJy beam}^{-1}$ per $\sim 15.5 \text{ km s}^{-1}$ channel. Upon binning the line-free channels, we obtain an rms noise of $0.03 \text{ mJy beam}^{-1}$ in the continuum map.

2.2. VLA observations

Radio continuum observations covering EGS141912 have been conducted using the NSF’s Karl G. Jansky Very Large Array (VLA) over 3 epochs in July–September 2013 (Program IDs 13B-289 and 13A-449). Observations were made in dual polarization using the X-band receivers in the C and CnB array configurations, with a 2 GHz bandwidth (7.988 – 9.884 GHz) sampled at a spectral resolution of 1 MHz. The total on-source time was 2.5 hours. 3C295 and J1419+5423 were used for absolute flux and phase calibration, respectively.

The VLA reduction pipeline in CASA v5.0.0 was used to flag and calibrate the observations. The weights for the visibilities were calculated using STATWT for the reduced measurement sets from each observational epoch, and they were combined into a single measurement set using the task CONCAT. The final measurement set was imaged and cleaned using the CASA task TCLEAN, using natural weighting to maximize point source sensitivity, and a pixel size of $0.''5 \times 0.''5$. Primary beam correction was applied during the cleaning process. All channels were binned together during cleaning. The resulting cleaned image has an rms noise of $1.3 \mu\text{Jy beam}^{-1}$ over the entire 2 GHz bandwidth, and a synthesized beam size of $3.''1 \times 2.''3$ (PA: -76°).

3. RESULTS

3.1. CO observations

We detect CO(5 – 4) emission from EGS141912 at $\sim 6\sigma$ significance, where the moment-0 emission map (Fig. 1) is created by binning the CO(5 – 4) line over the same velocities as the CO(3 – 2) emission in G17¹.

Based on a 2-D Gaussian fitting to the moment-0 map, we find a velocity integrated line flux of $I_{\text{CO}(5-4)} = 0.72 \pm 0.12 \text{ Jy km s}^{-1}$. This corresponds to a line luminosity of $L'_{\text{CO}(5-4)} = (1.3 \pm 0.2) \times 10^{10} \text{ K km s}^{-1} \text{ pc}^{-2}$. Both CO(3 – 2) and CO(5 – 4) spectra are extracted from a circular aperture with radius $1.0''$ centred on the position in Table 2 in order to compare their line profiles, though we caution that this corresponds to a small

fraction of the beam for the CO(3 – 2) cube, given its $\sim 4\times$ coarser spatial resolution (see Fig. 1). We do not detect any continuum emission from EGS141912, giving a 3σ upper limit of $f_\lambda \leq 0.1 \text{ mJy}$ at $\lambda_{\text{obs}} = 2.2 \text{ mm}$.

We also create the rms-weighted average of the CO(3 – 2) and CO(5 – 4) spectra (Fig. 1) and detect the combined emission at a $\sim 8\sigma$ significance, resulting in an improved $z_{\text{spec}} = 3.2185 \pm 0.0002$. The total gas mass has been derived using the CO(3 – 2) line (as in G17) and the line luminosities are listed in Table 2.

3.2. Radio continuum observations

We do not detect 9 GHz radio continuum emission from EGS 141912 at the spatial position of the CO emission, and find a 3σ upper limit of $f_{9\text{GHz}} \lesssim 3.9 \mu\text{Jy}$ ². We use this limit to constrain the 1.4 GHz luminosity ($L_{1.4\text{GHz}}$) as follows

$$L_{1.4\text{GHz}} = \frac{4\pi D_L^2}{(1+z)^{1+\alpha}} \left(\frac{1.4}{\nu_{\text{obs}}}\right)^\alpha S_{\nu_{\text{obs}}} \quad (1)$$

where D_L is the luminosity distance in metres, z is the source redshift, $\nu_{\text{obs}} \sim 9 \text{ GHz}$, and α is the radio spectral slope of $\alpha = -0.7$ (such that $S_\nu \propto \nu^\alpha$). This gives a 3σ upper limit on the 1.4 GHz luminosity of $L_{1.4\text{GHz}} \lesssim 8.7 \times 10^{23} \text{ W Hz}^{-1}$.

3.3. SED fitting

To obtain the stellar mass, we adopt the spectral energy distribution (SED) fitting package Code for Investigating GALaxy Emission (CIGALE ; Burgarella et al. 2005; Noll et al. 2009; Serra et al. 2011 as described in G17 with minor changes (see Appendix A for more details). We here only use those photometric data points where the emission is detected at $\text{SNR} \gtrsim 2$ as well as the upper limits on continuum emission based on our CO observations. The best-fit SED is shown in Figure 2, and the results of the SED fitting as well as all source properties are listed in Table 2. Based on the stellar mass based on the SED fit and gas mass based on the CO(3 – 2) line strength, we find a gas mass fraction $f_{\text{gas}} = M_{\text{gas}}/(M_{\text{gas}} + M_*) = 0.9 \pm 0.2$. The quoted uncertainty in the gas fraction does not include the systematic uncertainty associated with the stellar mass estimate due to assumptions about the star-formation history ($\sim 30\%$, see Appendix A), the uncertainties in the CO line luminosity ratio $L'_{\text{CO}(3-2)}/L'_{\text{CO}(1-0)}$, assumed to be $r_{31} = 0.42 \pm 0.07$ based on Daddi et al. (2015), or

¹ We do not fit a 1-D Gaussian to the CO(5 – 4) spectral line profile, as the line was observed close to the edge of the spectral band and we lack continuum coverage on one side of the band.

² We assume that the emission is not spatially resolved in the X-band observations, as it is not resolved in the CO(5 – 4) emission, observed with a similar beam size.

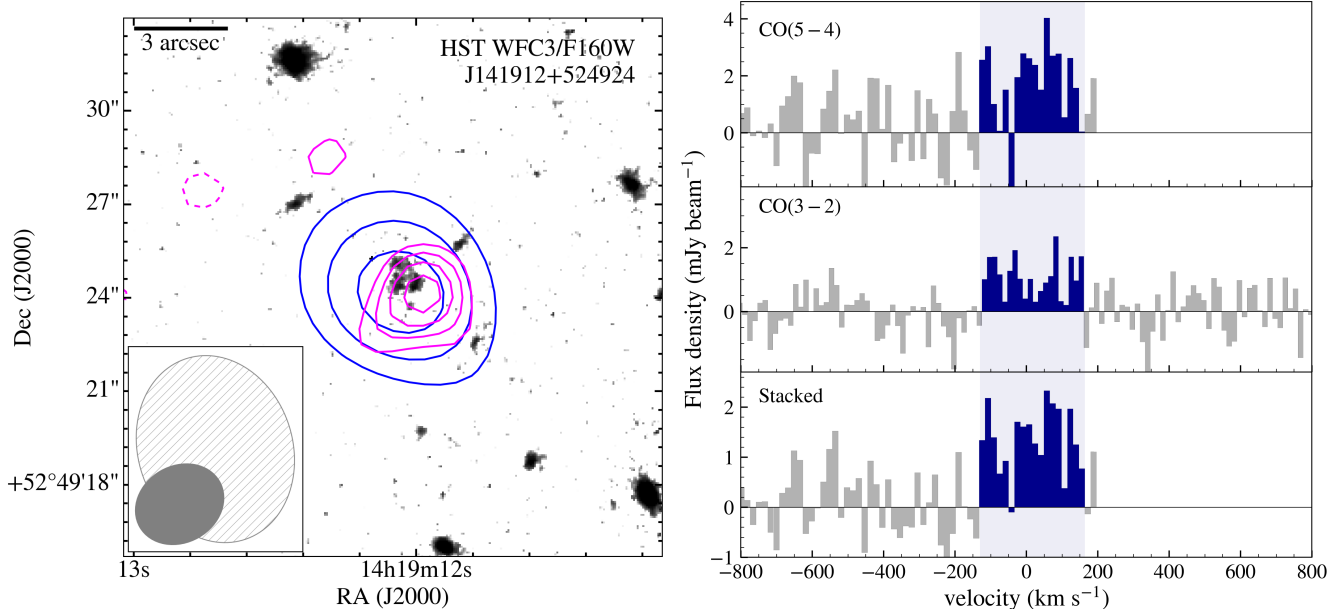


Figure 1. *Left:* HST/WFC3 F160W image for EGS141912 (Momcheva et al. 2015) with integrated CO(3 – 2) and CO(5 – 4) moment-0 emission shown as the blue and pink contours respectively. Contours are marked at the $\pm 3, 4, 5, 6\sigma$ levels, at $0.1 \text{ Jy km s}^{-1} \text{ beam}^{-1}$ for both maps. *Right:* CO(3 – 2) and CO(5 – 4) spectra (histograms) from a $1.0''$ aperture, as well as their weighted average spectrum. The moment-0 maps were made by summing the channels between $v \in (-130, 164) \text{ km s}^{-1}$, for which the velocity range was determined based on the detected emission in the rms-weighted stacked spectrum of the CO(3 – 2) and CO(5 – 4) spectra.

systematic uncertainties in the CO-H₂ gas mass conversion factor α_{CO} (see Bolatto et al. 2013 for a review).

There are large uncertainties associated with the L_{IR} for EGS141912. This is best demonstrated in Figure 2, where we compare the best-fit SED from CIGALE to high- z SED templates, both for normal and starburst galaxies (Magdis et al. 2012)³. It is clear that in the absence of photometry sampling the peak of the IR emission, the shape of the SED - and therefore the integrated L_{IR} - is poorly constrained. Physically, this arises because a mixed dust/star system may look identical to a dimmer, dust-free system at optical/UV wavelengths, and the two can be distinguished only using far-IR photometry. This lack of far-IR coverage also results in relatively poorly constrained dust mass obtained through SED fitting, $M_{\text{dust}} = (6.4 \pm 4.7) \times 10^8 M_{\odot}$ (also see Berta et al. 2016). This corresponds to a gas-to-dust mass ratio of $\delta_{\text{GDR}} = 400 \pm 300$, which is higher than but consistent with the expected $\delta_{\text{GDR}} \sim 100$ for solar metallicities (Leroy et al. 2011) within the uncertainties.

Anchoring SED templates for $z \sim 3$ main-sequence galaxies to the $24\mu\text{m}$ flux (Magdis et al. 2012), we infer an IR luminosity of $L_{\text{IR}}^{\text{MS}} = (2.1 \pm 0.3) \times 10^{12} L_{\odot}$. To get an upper limit on the L_{IR} , we fit the upper limit

on the NOEMA 2mm continuum flux with a Modified Blackbody function combined with a power-law mid-IR emission (see Pavesi et al. 2016, for details). We here assume an uniform prior on the dust temperature of $T_{\text{dust}} = 35 \pm 10 \text{ K}$ (as suitable for $z \sim 3$ galaxies, Magnelli et al. 2014) and a dust emissivity of $\beta = 1.7 \pm 0.2$ (Planck Collaboration et al. 2014). We find an upper limit of $L_{\text{IR}} \lesssim 4.8 \times 10^{12} L_{\odot}$ with a 99.7% confidence limit. Overall, we treat the L_{IR} as lying between the $L_{\text{IR}}^{\text{lower}} = 2.1 \times 10^{12} L_{\odot}$ and $L_{\text{IR}}^{\text{upper}} = 4.8 \times 10^{12} L_{\odot}$. These limits on the L_{IR} are consistent with those derived using the upper limit on the 1.4 GHz luminosity $L_{1.4\text{GHz}}$ when assuming a redshift-dependent radio-IR correlation⁴ (Delhaize et al. 2017). We find $q_{\text{IR}} \sim 2.2$ for $z \sim 3.2$ (assuming $\alpha = -0.7$) as compared to $q_{\text{IR}} \sim 2.6$ for a non-evolving radio-IR correlation (see Fig 3 Molnár et al. 2018). These correspond to upper limits on the $L_{\text{IR}} \lesssim 1.4 \times 10^{12} L_{\odot}$ and $L_{\text{IR}} \lesssim 3.4 \times 10^{12} L_{\odot}$, respectively.

We use the limits on L_{IR} to get limits for the $\text{SFR}_{\text{IR}} = 1.09 \times 10^{-10} L_{\text{IR}}$ (Chabrier 2003), finding $\text{SFR}_{\text{IR}} =$

⁴ The evolution of q_{IR} is an open question, with some studies finding a weak redshift evolution (Magnelli et al. 2015; Calistro Rivera et al. 2017; Delhaize et al. 2017), and with others finding differential evolution for disc- vs spheroid- dominated galaxies (Molnár et al. 2018).

³ <http://georgiosmagdis.pbworks.com/w/page-revisions/59019974/SED%20Templates>

Table 1. Continuum fluxes for EGS141912.

Telescope	Band	λ_{eff} (μm)	Flux (mJy)	Ref
CFHTLS	r'	0.63	$(3.6 \pm 1.4) \times 10^{-5}$	(1)
	i'	0.77	$(9.0 \pm 1.8) \times 10^{-5}$	(1)
HST	F606W	0.59	$(5.3 \pm 2.2) \times 10^{-5}$	(1)
	F814W	0.83	$(7.7 \pm 3.4) \times 10^{-5}$	(1)
	F125W	1.25	$(1.2 \pm 0.3) \times 10^{-4}$	(1)
	F140W	1.39	$(2.1 \pm 0.4) \times 10^{-4}$	(1)
	F160W	1.54	$(2.8 \pm 0.3) \times 10^{-4}$	(1)
Spitzer	IRAC	3.6	$(2.0 \pm 0.3) \times 10^{-3}$	(2)
	IRAC	4.5	$(2.5 \pm 0.5) \times 10^{-3}$	(2)
	IRAC	5.8	$(7.0 \pm 1.0) \times 10^{-3}$	(2)
	IRAC	8.0	$(2.6 \pm 1.2) \times 10^{-3}$	(2)
	MIPS	23.7	$(5.0 \pm 0.7) \times 10^{-2}$	(2)
Herschel	PACS	160	$(1.8 \pm 0.7) \times 10^1$	(3)
NOEMA		2.2×10^3	< 0.1	(4)
		3.7×10^3	< 0.3	(5)
VLA		3.4×10^4	$< 3.9 \times 10^{-3}$	(5)

References—(1) 3D-HST AEGIS catalog [Brammer et al. \(2012\)](#); [Skelton et al. \(2014\)](#), (2) [Park et al. \(2010\)](#) (3) [Oliver et al. \(2012\)](#) (4) G17 (5) This work.

$230 - 520 M_{\odot} \text{ yr}^{-1}$. EGS141912 then has a specific star-formation rate of $\text{sSFR} = 7.6 - 17.4 \text{ Gyr}^{-1}$ and gas depletion timescales of $\tau_{\text{dep}} = 1.1 - 0.5 \text{ Gyr}$. The sSFR is thus $0.9 - 2.1 \times \text{sSFR}_{\text{MS}}$, where sSFR_{MS} is the sSFR expected from a galaxy lying on the MS at $z \sim 3.2$ ([Speagle et al. 2014](#); [Tacconi et al. 2018](#)). EGS141912 is therefore consistent with the MS at $z \sim 3.2$.

4. DISCUSSION

4.1. CO excitation at $z \sim 3$

In general, the CO excitation (measured by line luminosity ratio between high- J and low- J CO lines) is expected to increase at higher- z due to the increased dust temperature ([Magdis et al. 2012](#)), and potentially due to higher dense gas fractions and star formation efficiencies (e.g. [Daddi et al. 2010](#); [Scoville et al. 2016](#)). Such a warm, highly excited molecular gas component is also expected based on simulations of gas excitation and feedback at higher redshifts (e.g. [Narayanan & Krumholz 2014](#); [Bournaud et al. 2015](#)). We here quantify the CO excitation in EGS141912 using the CO(3–2) and CO(5–4) line detections. For EGS141912, we

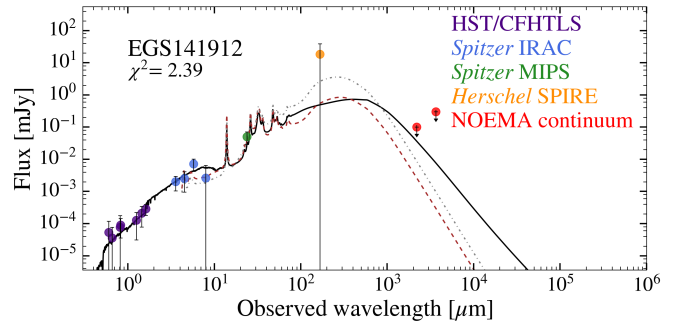


Figure 2. Results from SED-fitting for EGS141912 using CIGALE. The colored points represent the observed photometry, listed in [Table 1](#), and the gray line represents the best-fit SED. The far-IR tail of the SED is poorly constrained due to the lack of available photometry at those wavelengths. The dashed and dash-dotted lines show the fit using [Magdis et al. \(2012\)](#) templates for main-sequence ($z \sim 3$) and starburst galaxies.

Table 2. Physical properties of EGS141912

RA, Dec (J2000)	$14^{\text{h}} 19^{\text{m}} 12.0^{\text{s}} + 52^{\text{d}} 49^{\text{m}} 24^{\text{s}}$
z_{CO}	3.2185 ± 0.0002
L_{IR}	$2.1 - 4.8 \times 10^{12} L_{\odot}$
$L'_{\text{CO}(3-2)}$	$(3.0 \pm 0.5) \times 10^{10} \text{ K km s}^{-1} \text{ pc}^2$
$L'_{\text{CO}(5-4)}$	$(1.3 \pm 0.2) \times 10^{10} \text{ K km s}^{-1} \text{ pc}^2$
SFR_{IR}	$(230 - 520) M_{\odot} \text{ yr}^{-1}$
r_{53}	0.41 ± 0.10
M_{\star}	$(3.0 \pm 0.1) \times 10^{10} M_{\odot}$
$M_{\text{gas}}^{\text{a}}$	$(2.6 \pm 0.4) \times 10^{11} M_{\odot}$
M_{dust}	$(6.4 \pm 4.7) \times 10^8 M_{\odot}$
δ_{GDR}	400 ± 300
f_{gas}	0.9 ± 0.2
sSFR	$7.6 - 17.4 \text{ Gyr}^{-1}$

^aWe adopt the total molecular gas mass of $M_{\text{gas}} = (2.6 \pm 0.4) \times 10^{11} M_{\odot}$, as reported in [G17](#), calculated using $L'_{\text{CO}(3-2)}$, assuming a line luminosity ratio of $r_{31} = 0.42$ (the average from the [Daddi et al. 2015](#) sample of $z \sim 1.5$ BzK galaxies) and a CO-H₂ gas mass conversion factor $\alpha_{\text{CO}} = 3.6 M_{\odot} (\text{K km s}^{-1} \text{ pc}^2)^{-1}$, suitable for main-sequence galaxies at high redshift ([Daddi et al. 2010](#); [Carleton et al. 2017](#)).

find a line luminosity ratio of $L'_{\text{CO}(5-4)}/L'_{\text{CO}(3-2)} = 1.3 \pm 0.2/3.0 \pm 0.5 = 0.41 \pm 0.10$. This is slightly lower than but consistent with the excitation observed for BzK galaxies ($L'_{\text{CO}(5-4)}/L'_{\text{CO}(3-2)} = 0.53 \pm 0.19$; [Daddi et al. 2010, 2015](#)), and is lower than the observed excitation in submillimetre galaxies (SMGs; $r_{53} = 0.61 \pm 0.20$; [Bothwell et al. 2013](#)).

The star-formation efficiency in EGS141912 ($L_{\text{IR}}/M_{\text{gas}} \sim (8.1 - 18.4) L_{\odot}/M_{\odot}$) is also consistent with those ob-

served in BzK galaxies ($L_{\text{IR}}/M_{\text{gas}} \sim (13 \pm 3)L_{\odot}/M_{\odot}$ Daddi et al. 2015).

4.2. The CO-LIR correlation

CO(5–4) emission is a tracer of warm and dense molecular gas. $L'_{\text{CO}(5-4)}$ has been observed to correlate linearly with star formation rates and with L_{IR} in galaxies ranging from local spirals and (U)LIRGs to high- z star-forming galaxies, SMGs and QSOs (e.g. Liu et al. 2015; Daddi et al. 2015; Yang et al. 2017). This correlation is somewhat indirectly driven, as the CO emission arises from warm molecular gas, potentially partially heated by mechanical feedback and winds from star-forming regions. A similar correlation also exists between the $L'_{\text{CO}(3-2)}$ and the L_{IR} (see Fig. 3). The observed $L'_{\text{CO}(5-4)}$ and $L'_{\text{CO}(3-2)}$ are consistent with these relations within the scatter.

4.3. Evolution of the cosmic gas fraction

The gas fraction f_{gas} in galaxies is a function of M_* , sSFR/sSFR_{MS}, and z , with an increasing gas fraction at higher redshift, lower M_* , and in galaxies having lying above the MS (e.g. Bouché et al. 2010; Davé et al. 2011; Saintonge et al. 2011, 2012, 2017; Scoville et al. 2017; Tacconi et al. 2018). We use the function for this evolution given by Scoville et al. (2017):

$$f_{\text{gas}} = (1.0 + (1.41 \pm 0.18) \times (1.0 + z)^{-1.84 \pm 0.14} \times (\text{sSFR}/\text{sSFR}_{\text{MS}})^{-0.32 \pm 0.06} \times (M_*/10^{10} M_{\odot})^{0.70 \pm 0.04})^{-1}. \quad (2)$$

We compare this against the gas fraction obtained for EGS141912 in Fig. 4. For a MS galaxy at $z \sim 3.2$ with a stellar mass of $M_* = 3 \times 10^{10} M_{\odot}$, the expected gas fraction is $f_{\text{gas}} = 0.82$ for sSFR/sSFR_{ms} = 1.0, and $f_{\text{gas}} = 0.85$ for sSFR/sSFR_{ms} = 2.0. EGS141912 shows a gas fraction of $f_{\text{gas}} = M_{\text{gas}}/(M_* + M_{\text{gas}}) = 0.9 \pm 0.2$, which falls within a 99.7% confidence interval of the above relation. Similarly high gas fractions have been found in two MS galaxies at $z \sim 2 - 2.5$ (Tacconi et al. 2013; Decarli et al. 2016a), with one showing comparable M_* and M_{gas} to EGS141912, and the other having a significantly lower stellar mass ($M_* = 6 \times 10^9 M_{\odot}$; Tacconi et al. 2013).

5. CONCLUSION

We have presented molecular gas observations of EGS141912, one of the highest redshift unlensed MS galaxies detected in CO to date. Our observations of the CO(3–2) and CO(5–4) emission reveal that the gas excitation is consistent with that seen in $z \sim 1.5$ BzK galaxies, although toward the low end. EGS141912 also

has a similar star formation efficiency as other high- z MS galaxies between $z \sim 1.5 - 2.5$. We find EGS141912 to be gas-rich, with a gas fraction of $f_{\text{gas}} \sim 0.9 \pm 0.2$, which is consistent with scaling relations for the gas fraction of MS galaxies derived using dust-based measurements of the total ISM mass (Scoville et al. 2017). The uncertainties on the star formation efficiency and gas fraction for EGS141912 are driven by those on α_{CO} , L_{IR} and the unknown gas excitation, and we need both high spatial resolution observations of the CO(1–0) emission as well as observations at the peak of the far-IR SED to improve our knowledge of the cold molecular gas, the molecular gas fraction and its star-formation efficiency. EGS141912 lies well within the attained CO sensitivities by blind surveys such as ASPECS-Pilot (Decarli et al. 2016a,b; Walter et al. 2016) and COLDz (Pavesi et al. 2018; Riechers et al. 2019).

While most gas-rich galaxies in the universe at $z > 2$ have optical/IR counterparts (Tacconi et al. 2013; Decarli et al. 2016a; Pavesi et al. 2018), our findings for EGS141912 show that some of the most gas-rich systems would not be *preferentially* selected for targeted CO follow-up studies at high redshift, either based on optical or far-IR selection criteria (e.g. PHIBBS, Tacconi et al. 2013). Molecular line scan surveys such as COLDz and ASPECS, which by design are ideal for picking up galaxies like EGS141912, thus provide a complementary probe of the distant universe, and thus, significantly contribute towards our understanding of the total cold gas content throughout cosmic history (e.g., Decarli et al. 2016a; Riechers et al. 2019).

We thank the referee for excellent and helpful comments which have greatly improved the clarity of the work. A.G acknowledges support from the HST grant HST-GO-14938.003-A. D.R. and R.P acknowledge support from the National Science Foundation under grant number AST-1614213 to Cornell University. RP acknowledges support through the grant SOSPA3-008. This work is based on observations carried out under project number W16DR with the IRAM NOEMA Interferometer. IRAM is supported by INSU/CNRS (France), MPG (Germany) and IGN (Spain). This study makes use of data from AEGIS, a multiwavelength sky survey conducted with the Chandra, GALEX, Hubble, Keck, CFHT, MMT, Subaru, Palomar, Spitzer, VLA, and other telescopes and supported in part by the NSF, NASA, and the STFC. This work is based on observations taken by the 3D-HST Treasury Program (GO 12177 and 12328) with the NSAS/EST HST, which is operated by the Association of Universities for Research in Astronomy, Inc., under NASA contract NAS5-26555.

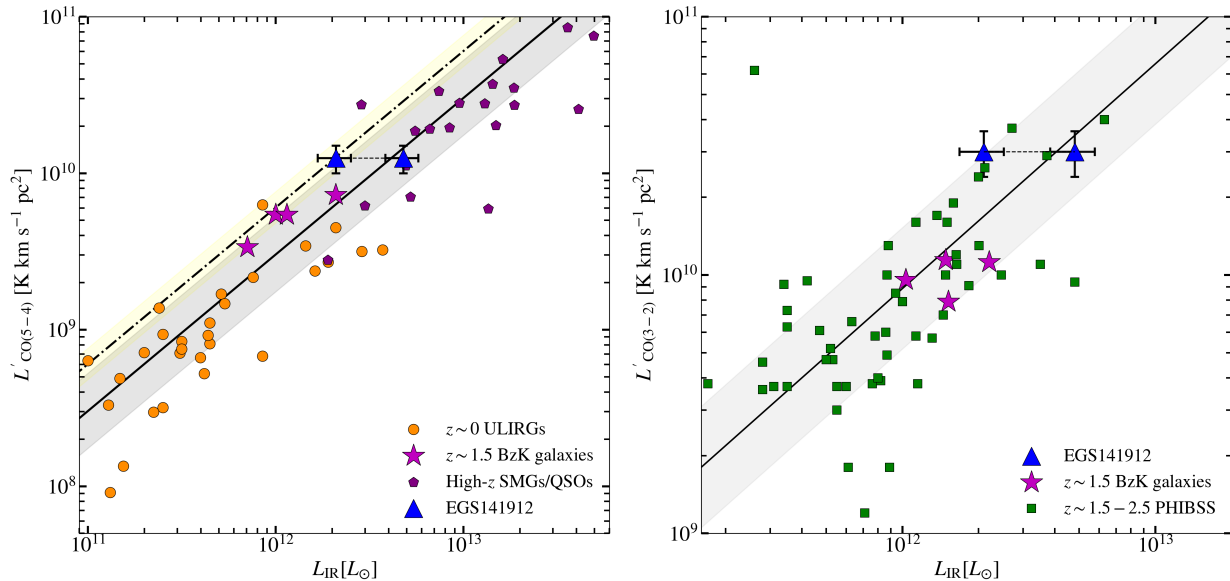


Figure 3. Left: A comparison of $L'_{\text{CO}(5-4)}$ vs L_{IR} for EGS141912 for galaxies including local (U)LIRGs, BzK galaxies, and high- z SMGs and QSOs. Right: $L'_{\text{CO}(3-2)}$ vs L_{IR} for star-forming galaxies observed at high- z (Tacconi et al. 2013; Daddi et al. 2015). The solid line and the dash-dotted line in the left panel show the best fit relations for all galaxies, and that for local spirals and LIRGs, respectively (Daddi et al. 2015). The solid line in the right panel shows the best fit for all galaxies including local spirals, (U)LIRGs, as well as high- z SMGs and QSOs (Sharon et al. 2016), assuming $\text{SFR} = 1.09 \times 10^{-10} L_{\text{IR}}$ based on a Chabrier IMF (Chabrier 2003). The shaded regions around each line show the 1σ deviation, assuming a constant slope.

The National Radio Astronomy Observatory is a facil-

ity of the National Science Foundation operated under cooperative agreement by Associated Universities, Inc.

APPENDIX

A. DETAILS OF SED MODELLING

We have used CIGALE to model the UV to IR SED of EGS141912. Although CIGALE can estimate a large number of galaxy physical properties (including dust attenuation, dust luminosity, M_* , SFR and L_{IR}), given the lack of far-IR photometry for EGS141912, we do not consider the L_{IR} and SFR estimates to be highly reliable (see § 3.3).

The modelling and estimation of uncertainties performed by CIGALE have been discussed in greater detail in Noll et al. (2009); Boquien et al. (2018), but we briefly describe them as follows. CIGALE uses independent modules for modelling star-formation histories (SFHs), stellar emission from different population synthesis models (Bruzual & Charlot 2003; Maraston 2005), dust attenuation (Calzetti et al. 2000), dust emission (e.g. Draine & Li 2007) and radio emission, which together create an integrated SED template. The code implicitly maintains energy balance between the UV attenuation and dust emission. CIGALE takes a range of parameters for each of these modules as input, and builds a model for each combination of parameters. After the grid of normalized models is computed. The models are scaled and compared against the provided photometry, CIGALE finds a likelihood for each of the models, defined as $e^{-\chi^2}$. These likelihoods are used to compute the likelihood-weighted mean of the physical parameters and their likelihood-weighted uncertainties, which are returned as the best-fit parameters.

We here focus on the uncertainties on the stellar mass M_* . For EGS141912, we find a stellar mass of $M_* = (3.0 \pm 0.1) \times 10^{10} M_{\odot}$, assuming a delayed exponential star-formation history, and the Bruzual & Charlot (2003) stellar population synthesis model. To test how robust M_* is to our choice of SFH, we have explored the different possible SFHs allowed by CIGALE - a double exponential, a delayed star-formation, as well as a periodic bursts of star-formation. We find a $\sim 30\%$ variation in M_* assuming different models, with $M_* = (3.0 \pm 0.1) \times 10^{10} M_{\odot}$ for a delayed exponential SFH, to $M_* = (3.9 \pm 0.5) \times 10^{10} M_{\odot}$ for periodic bursts of star formation. Assuming a delayed SFH results in the fit with the lowest reduced $\chi^2 \sim 2.3$, as compared to $\chi^2 \sim 2.7$ and $\chi^2 \sim 3.0$ for double exponential SFH and a periodic SFH, respectively. We therefore assume a delayed SFH for the final best-fit SED.

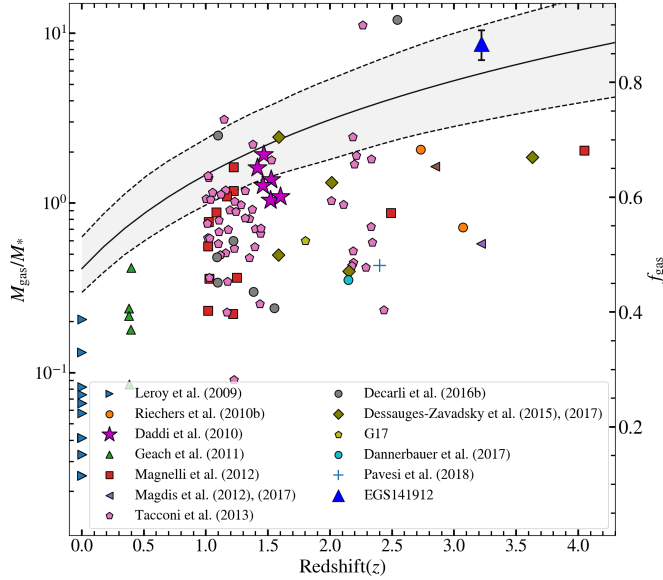


Figure 4. The ratio of molecular gas mass to stellar mass (calculated using an $\alpha_{\text{CO}} \sim 3.6 M_{\odot} (\text{K km s}^{-1} \text{pc}^{-2})^{-1}$ for all sources) adapted from Carilli & Walter (2013). Previous observations are from Leroy et al. (2009); Riechers et al. (2010); Daddi et al. (2010); Geach et al. (2011); Magnelli et al. (2012); Magdis et al. (2012); Tacconi et al. (2013); Dessauges-Zavadsky et al. (2015); Decarli et al. (2016a); Dessauges-Zavadsky et al. (2017); Dannerbauer et al. (2017); Gowardhan et al. (2017); Pavese et al. (2018). The black line shows the scaling relation between f_{gas} and z , assuming a stellar mass of $M_{*} = 3 \times 10^{10} M_{\odot}$ and $\text{sSFR} = 2\text{sSFR}_{\text{MS}}$; the shaded regions show the 99.7% confidence regions. EGS141912 is consistent with an increasing gas fraction at $z \gtrsim 3$.

REFERENCES

- Berta, S., Lutz, D., Genzel, R., Förster-Schreiber, N. M., & Tacconi, L. J. 2016, *A&A*, 587, A73
- Béthermin, M., Daddi, E., Magdis, G., et al. 2015, *A&A*, 573, A113
- Bolatto, A. D., Wolfire, M., & Leroy, A. K. 2013, *ARA&A*, 51, 207
- Boquien, M., Burgarella, D., Roehlly, Y., et al. 2018, arXiv e-prints, arXiv:1811.03094
- Bothwell, M. S., Smail, I., Chapman, S. C., et al. 2013, *MNRAS*, 429, 3047
- Bouché, N., Dekel, A., Genzel, R., et al. 2010, *ApJ*, 718, 1001
- Bournaud, F., Daddi, E., Weiß, A., et al. 2015, *A&A*, 575, A56
- Brammer, G. B., van Dokkum, P. G., Franx, M., et al. 2012, *ApJS*, 200, 13
- Bruzual, G., & Charlot, S. 2003, *MNRAS*, 344, 1000
- Burgarella, D., Buat, V., & Iglesias-Páramo, J. 2005, *MNRAS*, 360, 1413
- Calistro Rivera, G., Williams, W. L., Hardcastle, M. J., et al. 2017, *MNRAS*, 469, 3468
- Calzetti, D., Armus, L., Bohlin, R. C., et al. 2000, *ApJ*, 533, 682
- Carilli, C. L., & Walter, F. 2013, *ARA&A*, 51, 105
- Carleton, T., Cooper, M. C., Bolatto, A. D., et al. 2017, *MNRAS*, 467, 4886
- Chabrier, G. 2003, *ApJ*, 586, L133
- Coppin, K. E. K., Swinbank, A. M., Neri, R., et al. 2007, *ApJ*, 665, 936
- Daddi, E., Bournaud, F., Walter, F., et al. 2010, *ApJ*, 713, 686
- Daddi, E., Dannerbauer, H., Liu, D., et al. 2015, *A&A*, 577, A46
- Danielson, A. L. R., Swinbank, A. M., Smail, I., et al. 2011, *MNRAS*, 410, 1687
- Dannerbauer, H., Lehnert, M. D., Emonts, B., et al. 2017, *A&A*, 608, A48

- Davé, R., Finlator, K., & Oppenheimer, B. D. 2011, *MNRAS*, 416, 1354
- Decarli, R., Walter, F., Aravena, M., et al. 2016a, *ApJ*, 833, 70
- . 2016b, *ApJ*, 833, 69
- Delhaize, J., Smolčić, V., Delvecchio, I., et al. 2017, *A&A*, 602, A4
- Dessauges-Zavadsky, M., Zamojski, M., Schaerer, D., et al. 2015, *A&A*, 577, A50
- Dessauges-Zavadsky, M., Zamojski, M., Rujopakarn, W., et al. 2017, *A&A*, 605, A81
- Draine, B. T., & Li, A. 2007, *ApJ*, 657, 810
- Geach, J. E., Smail, I., Moran, S. M., et al. 2011, *ApJ*, 730, L19
- Genzel, R., Tacconi, L. J., Lutz, D., et al. 2015, *ApJ*, 800, 20
- Gowardhan, A., Riechers, D. A., Daddi, E., et al. 2017, *ApJ*, 838, 136
- Lagos, C. D. P., Baugh, C. M., Lacey, C. G., et al. 2011, *MNRAS*, 418, 1649
- Leroy, A. K., Walter, F., Bigiel, F., et al. 2009, *AJ*, 137, 4670
- Leroy, A. K., Bolatto, A., Gordon, K., et al. 2011, *ApJ*, 737, 12
- Liu, D., Gao, Y., Isaak, K., et al. 2015, *ApJL*, 810, L14
- Magdis, G. E., Daddi, E., Sargent, M., et al. 2012, *ApJL*, 758, L9
- Magdis, G. E., Rigopoulou, D., Daddi, E., et al. 2017, *A&A*, 603, A93
- Magnelli, B., Saintonge, A., Lutz, D., et al. 2012, *A&A*, 548, A22
- Magnelli, B., Lutz, D., Saintonge, A., et al. 2014, *A&A*, 561, A86
- Magnelli, B., Ivison, R. J., Lutz, D., et al. 2015, *A&A*, 573, A45
- Maraston, C. 2005, *MNRAS*, 362, 799
- Molnár, D. C., Sargent, M. T., Delhaize, J., et al. 2018, *MNRAS*, 475, 827
- Momcheva, I. G., Brammer, G. B., van Dokkum, P. G., et al. 2015, *ArXiv e-prints*, arXiv:1510.02106
- Narayanan, D., & Krumholz, M. R. 2014, *MNRAS*, 442, 1411
- Noll, S., Burgarella, D., Giovannoli, E., et al. 2009, *A&A*, 507, 1793
- Obreschkow, D., & Rawlings, S. 2009, *ApJL*, 696, L129
- Oliver, S. J., Bock, J., Altieri, B., et al. 2012, *MNRAS*, 424, 1614
- Park, S. Q., Barmby, P., Willner, S. P., et al. 2010, *ApJ*, 717, 1181
- Pavesi, R., Riechers, D. A., Capak, P. L., et al. 2016, *ApJ*, 832, 151
- Pavesi, R., Sharon, C. E., Riechers, D. A., et al. 2018, *ApJ*, 864, 49
- Planck Collaboration, Ade, P. A. R., Aghanim, N., et al. 2014, *A&A*, 564, A45
- Riechers, D. A., Carilli, C. L., Walter, F., & Momjian, E. 2010, *ApJL*, 724, L153
- Riechers, D. A., Hodge, J., Walter, F., Carilli, C. L., & Bertoldi, F. 2011a, *ApJL*, 739, L31
- Riechers, D. A., Walter, F., Carilli, C. L., et al. 2006, *ApJ*, 650, 604
- Riechers, D. A., Carilli, C. L., Maddalena, R. J., et al. 2011b, *ApJL*, 739, L32
- Riechers, D. A., Bradford, C. M., Clements, D. L., et al. 2013, *Nature*, 496, 329
- Riechers, D. A., Pavesi, R., Sharon, C. E., et al. 2019, *ApJ*, 872, 7
- Rodighiero, G., Daddi, E., Baronchelli, I., et al. 2011, *ApJL*, 739, L40
- Saintonge, A., Kauffmann, G., Wang, J., et al. 2011, *MNRAS*, 415, 61
- Saintonge, A., Tacconi, L. J., Fabello, S., et al. 2012, *ApJ*, 758, 73
- Saintonge, A., Lutz, D., Genzel, R., et al. 2013, *ApJ*, 778, 2
- Saintonge, A., Catinella, B., Tacconi, L. J., et al. 2017, *The Astrophysical Journal Supplement Series*, 233, 22
- Schinnerer, E., Groves, B., Sargent, M. T., et al. 2016, *ApJ*, 833, 112
- Scoville, N., Sheth, K., Aussel, H., et al. 2016, *ApJ*, 820, 83
- Scoville, N., Lee, N., Vanden Bout, P., et al. 2017, *ApJ*, 837, 150
- Serra, P., Amblard, A., Temi, P., et al. 2011, *ApJ*, 740, 22
- Sharon, C. E., Riechers, D. A., Hodge, J., et al. 2016, *ApJ*, 827, 18
- Skelton, R. E., Whitaker, K. E., Momcheva, I. G., et al. 2014, *ApJS*, 214, 24
- Speagle, J. S., Steinhardt, C. L., Capak, P. L., & Silverman, J. D. 2014, *ApJS*, 214, 15
- Spergel, D. N., Bean, R., Doré, O., et al. 2007, *ApJS*, 170, 377
- Strandet, M. L., Weiss, A., De Breuck, C., et al. 2017, *ApJ*, 842, L15
- Tacconi, L. J., Neri, R., Genzel, R., et al. 2013, *ApJ*, 768, 74
- Tacconi, L. J., Genzel, R., Saintonge, A., et al. 2018, *ApJ*, 853, 179
- Tan, Q., Daddi, E., Sargent, M., et al. 2013, *ApJ*, 776, L24
- Troncoso, P., Maiolino, R., Sommariva, V., et al. 2014, *A&A*, 563, A58

Walter, F., Decarli, R., Aravena, M., et al. 2016, ApJ, 833,
67

Weiß, A., Downes, D., Neri, R., et al. 2007, A&A, 467, 955

Weiß, A., Downes, D., Walter, F., & Henkel, C. 2005, A&A,
440, L45

Yang, C., Omont, A., Beelen, A., et al. 2017, A&A, 608,
A144